A POD BASED ANALYSIS OF THE 2D CYLINDER WAKE MODE INTERACTIONS

N. W. Mureithi [1], M. Rodriguez [2], P. Versailles, A. Pham, and H.D. Vo

Department of Mechanical Engineering,
École Polytechnique, Montréal, QC, Canada H3T 1J4

[1] *BWC/AECL/NSERC Chair of Fluid-Structure Interaction*

[2] *LadHyX, Ecole Polytechnique, 91128 Palaiseau, France*

ABSTRACT

The dynamic behavior of a cylinder wake at low Reynolds numbers is studied theoretically and experimentally. Theoretically, symmetry-group equivariant bifurcation theory is employed. Starting with a 2D CFD simulation of the transverse flow past a fixed cylinder, the most important Karman wake flow modes are derived via POD decomposition. From the known spatial symmetries of the first two modes, symmetry-equivariant bifurcation theory has been employed to derive the lowest order discrete dynamical system (amplitude equations) modeling the mode interactions in Poincare space. The CFD based POD modal data for the stationary cylinder is used to determine the coefficients of these amplitude equations. The paper presents an analysis of the wake dynamics based on the amplitude equations. It is found that the apparent complex wake dynamics can be predicted by the surprisingly simple Poincare map which yields the main bifurcations observed. Typical bifurcations including homoclinic and period-doubling, encountered in the classical Bogdanov-Takens scenario, are predicted and shown to agree reasonably well with CFD results.

Preliminary results of experimental tests on vortex-induced vibration control, motivated by the foregoing results, and testing new using plasma actuator technology, are also presented.

1. INTRODUCTION

Numerous vortex wake modes have been observed having different spatio-temporal symmetry and their transitions explain some of the observed wake phenomena. For example, as first observed by Williamson & Roshko (1988) and then confirmed by Brika & Laneville (1993,1995), the jump in the response amplitude which coincides with a half period (π) phase shift between the cylinder motion and the fluid force, is due to the transition, near resonance, from the *2S* mode of vortex shedding to the *2P* mode. Ongoren & Rockwell (1988) have also described a competition between different vortex wake modes. Spatial symmetry was found to be a key feature in the wake flow. This observation prompted Mureithi et al. (2002, 2005) to delve deeper into the implications of the observed wake symmetry in helping understand the underlying wake dynamics. A pair of simple discrete amplitude equations governing the nonlinear interaction of the Karman and reflection-symmetry modes were derived using symmetry equivariant bifurcation theory. A qualitative analysis of these equations showed that a number of standard bifurcations of the Karman mode could be expected as the amplitude of the reflection-symmetric mode was varied. Possible changes in the wake symmetry induced by increased forcing such as period-doubling or symmetry breaking in the cylinder wake in the case of streamwise harmonic forcing were predicted.

In more recent work, Rodriguez & Mureithi (2006) have performed CFD computations of the wake flow behind a cylinder undergoing periodic excitation in the flow direction. The role of spatial-temporal symmetry in the wake flow was elucidated by a POD analysis of the wake flow velocity field.

The POD modes derived in this work provide a new avenue for the analysis of the forced wake flow. In the present work, These modes are used to determine the unknown coupling coefficients in the discrete amplitude equations derived earlier. A more quantitative analysis of this low dimensional wake model therefore becomes possible.

2. CYLINDER WAKE DYNAMICS

2.1 Cylinder wake response to external forcing

The problem under study is that of a circular cylinder subjected to transverse flow at Re=1000. The flow is assumed to be two-dimensional. This assumption is reasonable in the case of forced cylinder motion which increases the effective correlation of flow structures along the cylinder span thus reducing three-dimensional effects. It should also be noted that the wake flow dynamics of interest in the present work are primarily two-dimensional. The validity of this assumption is

verified *a posteriori*. Numerical simulations were carried out using the CFD code Fluent. Details of the simulation parameters and verification of the numerical procedure may be found in Mureithi & Rodriguez (2005), Rodriguez & Mureithi (2006) and Rodriguez (2006). Simulations were all carried out during 10000 time steps. The last 5000 time steps were used to analyze the steady state flow downstream of the cylinder in the case of periodic responses. In the case of quasi-harmonic or chaotic responses, the last 5000 time steps were also used to analyze the flow with the same precision in frequency decomposition as in the case of the periodic responses.

The effect of cylinder stream-wise forcing on the wake flow has been studied in terms of vortex wake modes as a function of the cylinder oscillation amplitude. The inline forcing frequency corresponded to the Karman shedding frequency. Five response ranges were exhibited as the perturbation parameter was increased. For small cylinder amplitudes, up to *A/D*=0.075 (*D* being the cylinder diameter), the wake has a quasi-periodic response which turns to a chaotic response on increasing the amplitude. For *A/D*=0.15, the wake stabilizes in a periodic vortex shedding having a S configuration in Williamson & Roshko's (1988) terminology. At *A/D*=0.175, the wake destabilizes via symmetry breaking into a P+S configuration. This wake structure is shown in Fig.1(a) for *A/D*=0.25. For *A/D=0.35*, the wake stabilizes again in a S mode of vortex shedding but at shedding frequency half the Karman shedding frequency for the stationary cylinder, Fig.1(b).

From a dynamics point of view then, varying the cylinder forcing amplitude parameter triggers a sequence of bifurcations culminating in period-doubling. One of the primary goals of the present work was therefore to see if a simple discrete dynamical model based on symmetry group theory could reproduce this sequence of bifurcations, and in the process shed light on the underlying mechanisms for the observed changes in the wake.

2.2 POD wake modes

POD analysis based on the Karhunen-Loève decomposition was performed to extract the principal modes in the stream-wise velocity profile $u'(y,t)$ at locations 10*D* downstream of the cylinder. In the analysis, the flow field is projected onto an orthonormal set of functions $\Psi_k(y)$, (*topos*), each having time evolution $a_k(t)$ (*chronos*). The velocity profile may therefore be expressed as

$$u'(y,t) = \sum_{k=1}^{r} a_k(t)\Psi_k(y) \qquad (1)$$

The *chronos* magnitude represents the relative energy carried by the corresponding *topos*.

Fig.2 shows the first two *topos* modes of the x-velocity *u(y,t)* on the 10D line downstream of the cylinder. The modal decomposition clearly brings out the symmetry in the flow. This spatial-temporal symmetry may be conveniently described by normalizing the basic shedding wavelength to 2π. Defining the wavelength of the flow, λ, as shown in equation (2), helps characterize the spatio-temporal symmetry of the modes.

$$\lambda = \frac{U}{f_e} \equiv 2\pi \qquad (2)$$

Thus, respectively, the first three modes found in the fixed cylinder wake have $Z_2(\kappa,\pi)$, $D_2(\kappa,\pi)$ and $Z_2(\kappa,2\pi/3)$ symmetries. In this notation then, the Karman 2S mode symmetry is $Z_2(\kappa,\pi)$, meaning that the 2S mode is invariant by a composition of reflection (κ) and a translation downstream by half a period, see Fig.2(a). $D_2(\kappa,\pi)$ symmetry means the second mode is both invariant under reflection and under translation parallel to the flow by half a period. The symmetries of the other modes can be similarly described.

The P+S mode at *A/D*=0.25, Fig.1(b) may now be conveniently described more accurately by the symmetry group $Z_2(I,2\pi)$. This symmetry is a sub-group of $Z_2(\kappa,\pi)$. The flow has lost its reflection (κ) symmetry via (possibly) a pitchfork bifurcation leaving only a translation symmetry and double the shedding period.

3. MODE INTERACTION DYNAMICS

3.1 Derivation of reduced-order model

As is clear from the preceding sections, the periodically forced flow undergoes a series of well defined bifurcations.

The sequence of bifurcations in the wake dynamics can be conveniently represented in a reduced discrete Poincare space by plotting the discrete evolution of the real and imaginary parts of the initially (for stationary cylinder) $Z_2(\kappa,\pi)$-symmetric POD mode **K** amplitude.

The resulting bifurcations sequence is shown in Figure 3. Starting from the stable periodic (limit cycle) state for *A/D*=0, Fig.3(a), a quasi-periodic state is found near *A/D*=0.05, Fig. 3(b); the limit cycle appears to have undergone a symmetry-breaking bifurcation as well. Increasing the forcing amplitude, an apparently 'chaotic' state is found for forcing near *A/D*=0.1, Fig. 3(c). A further increase in forcing amplitude near *A/D*=0.35 results in a stable period-doubled state as seen in Fig.3(d).

In this section, an attempt is made to quantify (from a model dynamics point of view) the bifurcation sequence observed above. The bifurcation behavior is again studied in the reduced Poincaré space. To arrive at a tractable model discrete dynamical system we suppose

that the two lowest spatio-temporal modes dominate the dynamics. The two modes we consider are those for the unforced cylinder; the first two *topos* modes **K** and mode **S** shown in Fig.2. The spatial symmetries of these modes are, respectively, $\Gamma_K = Z_2(\kappa, \pi)$, and $\Gamma_S = D_2(\kappa, \pi)$. Since POD gives normalized *topos*, the amplitude evolution of the modes is contained in the *chronos*. Starting with the symmetries Γ_K and Γ_S, Mureithi et al. (2002) have employed equivariant bifurcation theory to derive the general form of the amplitude equations governing the interactions between modes **K** and **S**.

Representing the complex *(chronos)* mode amplitude by K and S, respectively, the discrete form of the mode amplitude interaction equations to third order is

$$K_{n+1} = \left(1 + \alpha_0 + \gamma_{11}|S_n|^2 + \alpha_2|K_n|^2\right)K_n + \delta_{01}S_n^2\overline{K}_n$$
$$S_{n+1} = \left(1 + \beta_0 + \beta_2|S_n|^2 + \gamma_{21}|K_n|^2\right)S_n + \mu_{01}\overline{S}_nK_n^2 \quad (3)$$

Equation (3) gives the general form of the amplitude equations given the symmetries Γ_K and Γ_S. To determine the (generally complex) constants $\alpha_k, \beta_k, \gamma_{kl}$ etc., the Poincaré reduction of the computed spatio-temporal mode data for A/D=0, Fig.3(a), are used. The data are first "complexified" via a Hilbert transform. The average wake period is used for discretization. **K** and **S** amplitudes are calculated for 45 wake shedding periods, thus the amplitude equations coefficients can be determined using a least square method to solve the over-determined system of equations. Constraints that restrain the amplitude equations, from a stability point of view were verified during the least-squares calculations. These constraints are given below.

$$\text{Re}(\alpha_0) > 0; \ \text{Re}(\alpha_2) < 0; \ \text{Re}(\beta_2) < 0; \ \text{Re}(\beta_0) > 0; \quad (4)$$

The constraints assure the stability of the modes in the case of no forcing. The map resulting when mode **S** is considered "constant" has $Z_2(\kappa, \pi)$ symmetry. The map and its complex conjugate are:

$$K_{n+1} = \left(\mu + \alpha_2|K_n|^2\right)K_n + \delta\overline{K}_n$$
$$\overline{K}_{n+1} = \left(\overline{\mu} + \overline{\alpha}_2|K_n|^2\right)\overline{K}_n + \delta K_n \quad (5)$$

where, $\mu = 1 + \alpha_0 + \gamma_{11}|S|^2$; $\delta = \delta_{01}S^2$.

3.2 Prediction of wake dynamics by reduced-order model

We consider now the dynamics of the **K** mode as the amplitude of the **S** mode is varied in the Poincare map (5). For the very low forcing (**S**) amplitudes, the limit cycle of Fig.3(a) is reproduced as expected as shown Fig.4(a). The limit cycle amplitude remains stable (albeit

changing shape) as S increases. Near S=0.32, a pitchfork bifurcation of the flow field occurs. The unstable fixed point (source) at the origin transforms into a saddle, while two symmetrically located unstable fixed points are created, Fig.4(b). As S is further increased, a subcritical Hopf bifurcation near S=0.33 leads to the creation of two unstable limit cycles. The unstable limit cycles disappear in a Homoclinic bifurcation. At the same time, a new large unstable limit cycle is created just inside the outer limit cycle, seen in Fig.4(c) for S=0.3325. When S is increased further the outer two limit cycles collide and disappear in a saddle node (fold) bifurcation, see Fig.4(d) for S=0.3375.

The bifurcation sequence described above is the classical Takens-Bogdanov bifurcation scenario. The hallmark of the Takens-Bogdanov bifurcation is the presence of double-zero eigenvalues for the reduced linearized system. We now compare the predicted bifurcation sequence with bifurcations observed in the numerical simulations. Two important remarks should be made, however. First, the reader is reminded that the **S** mode is treated as a parameter and is thus not affected by mode **K** in the simple reduced model. Second, the dynamical system of equation (5) has $Z_2(\kappa, \pi)$ symmetry. This symmetry must be considered for correct interpretation of the Takens-Bogdanov bifurcation sequence discussed above.

Qualitatively, the mapping (5) reproduces the observed bifurcations reasonably well. In the numerical computation, we start off in the cylinder fixed case with a closed curve on the K_r, K_i plane, Fig.3(a). This initial limit cycle results from the Hopf bifurcation responsible for the onset of vortex Karman shedding. For a forcing amplitude of A/D=0.05 the limit cycle has undergone a symmetry-breaking bifurcation. For the mapping (5), this was found to be a pitchfork bifurcation, Fig.4(b). A homoclinic bifurcation is predicted to occur next by the mapping (5). In the CFD based map, complex, possibly chaotic, behaviour is found for A/D=0.075 – 0.1. Homoclinic bifurcations are known to be an important precursor to chaos. We hypothesize that this is actually what happens in the higher dimensional fluid systems resulting in the Poincare map of Fig.3(c). The final state is a highly organized period-2 state as shown in Fig.3(d). The mapping (5) on the other hand predicts a pair of fixed point states appearing via a pitchfork bifurcation. As shown in the Appendix, the mapping (5) is the square of a second, lower order, mapping which is obtained when the presence of $\Gamma_K = Z_2(\kappa, \pi)$ symmetry is considered. A period-doubling bifurcation of this, more fundamental, lower order map translates into a pitchfork bifurcation in the squared mapping. In other words then, the mapping (5) does, in fact, predict the final period-doubling instability found in the cylinder wake for high amplitude forcing.

4. EXPERIMENTAL TESTS

The period-doubling bifurcation of the Karman mode, triggered by symmetrical forcing suggests an interesting idea for vibration control during Karman excitation.

Some preliminary experiments have been carried out to investigate the possibility of vibration control via induced flow bifurcation. The vortex shedding control experiments been carried out on a flexibly mounted cylinder having a 6.5 Hz natural frequency.

4.1 Test Cylinder and Plasma Actuators

The period-doubling bifurcation of the Karman mode is induced by the $D_2(\kappa,\pi)$-symmetric mode. To achieve this mode experimentally, plasma actuators were used. The actuators consist of a pair of electrodes separated by a non-conducting dielectric material running the length of the cylinder. The principle behind the actuator is fairly simple. As depicted in Fig.5, application of a radio-frequency high a.c. voltage across the electrodes ionizes the air in the region of the highest electric potential. Due to the existing electric field gradient, the charged ions are attracted towards the electrode of opposite charge creating a body force on the surrounding flow. In the tests reported here, a pair of actuators were installed on the test cylinder close to the upper and lower flow separation lines shown in Figure 6. The actuators create a jet having a maximum velocity of approximately 3 m/s depending on actuation voltage and frequency. In the tests, much lower jet velocities were needed.

4.2 Test Results

Tests were performed using a flexibly mounted cylinder having a natural frequency approximately 7 Hz. For the D=40.4mm diameter cylinder vortex-shedding resonance occurs at approximately U=1.5 m/s. Symmetric actuator pulsations with a pulse jet velocity ranging from 0.03 – 0.25 m/s, in the cylinder wake, were applied on the cylinder upper and lower surfaces near the flow separation lines. Due to cylinder curvature, the jet flow, in the near wake, is oriented towards the cylinder centerline as opposed to being parallel to the upstream flow.

Figure 7 shows examples of the wake velocity field for 0.03 m/s pulsations; the region immediately behind the cylinder and up to approximately 3D downstream is shown. Complex vortex-shedding is apparent. The pair of symmetrical vortices in Fig.7(a) later merge asymmetrically leading to an approximate P+S wake pattern. Frequency spectra for the inflow (u-) and transverse (v-) local flow velocities, at a location 1.4D downstream of the cylinder, are shown in Fig. 8(a) for 0.03 m/s jet velocity. The inflow velocity (u) component has a peak frequency component at 6 Hz corresponding to the jet pulsation frequency; pulsation was introduced near the vortex shedding frequency. The transverse velocity (v) component shows a dominant peak frequency at 3 Hz, which is half the forcing frequency. The Karman mode has therefore undergone a period-doubling bifurcation induced by the reflection symmetric jet forcing. The 3 Hz frequency component is even

stronger further downstream, at 2.4D downstream, as the instability develops spatially downstream as seen in Fig. 8(b).

This wake flow bifurcation has a strong effect on the vortex shedding-induced resonance. For 0.03 m/s jet velocity, the tube vibration amplitude is significantly reduced. When the jet velocity is increased to 0.25 m/s, the resonance is eliminated. Note that only a small amount of energy is expended to achieve control. This is due to the fact that energy is only used to trigger a bifurcation which leads to frequency detuning between fluid and structure. Vortex formation is still present but the wake frequency is no longer close to the structural frequency.

5. CONCLUSION

Symmetry-group equivariant bifurcation theory has been employed to derive employed to derive the lowest order discrete dynamical system modeling cylinder wake mode interactions in Poincare space. This surprisingly simple discrete map yields the main bifurcations observed in CFD simulations including homoclinic and period-doubling bifurcations. Preliminary results of experimental tests on Karman wake control using plasma actuators are also presented. Bifurcation control is shown to be potentially useful as a control strategy for vortex-induced vibrations.

6. ACKNOWLEDGEMENTS

7. APPENDIX

The solution of the equation

$$K_{n+1} = \Phi(K_n, \mu); \qquad \mu = \mu(S) \qquad (6)$$

yields the (flow) mapping

$$\Psi_{n_0}^n : C \to C; \; K_{n_0}(t_0) \to K_n(t_n), K \in C \qquad (7)$$

Using the normalized shedding period 2π, we define the Poincaré map from the flow $\Psi_{n_0}^n$,

$$\Psi_{pc} = \Psi^{2k\pi} \qquad (8)$$

Having arbitrarily set $n_0=0$. The mapping Ψ_{n0}^n is invariant under the symmetry operation $\Gamma_K = Z_2(\kappa,\pi)$. This means that

$$\Psi_{pc} = \Gamma[\Psi_{pc}] = \kappa \circ \Psi_{pc}^\pi \qquad (9)$$

Equation (9) has the consequence that the Poincaré mapping Ψ_{pc} is the square of the lower order mapping

$$\tilde{\Psi}_{pc} = \kappa \circ \Psi_{pc} = \Psi_{pc}^\pi, \qquad (9)$$

thus

$$\Psi_{pc} = \left(\tilde{\Psi}_{pc}\right)^2 \qquad (10)$$

The Poincaré maps presented in Figs.3 and 4 correspond to the mapping ψ_{pc} based on period $2k\pi$. Note also that the flow symmetry is restricted to $\Gamma_K = Z_2(\kappa, \pi)$ since the excitation mode S is reduced to a single amplitude parameter. Any $2k\pi$-periodic orbit will correspond to a fixed point of Ψ_{pc}. A symmetry-breaking bifurcation also yields a fixed point. However, the latter corresponds to a period-doubling for the lower order mapping $\tilde{\Psi}_{pc}$.

8. REFERENCES

Brika, D., Laneville, A., 1995, An experimental study of the aeolian vibrations of a flexible circular cylinder at different incidences. *Journal of Fluids and Structures*. 9:371-391.

Brika, D., Laneville, A., 1993, Vortex-induced vibrations of a long flexible circular cylinder. *Journal of Fluid Mechanics*. 250:481-508.

Mureithi, N.W., et al., 2002, Symmetry breaking and mode interaction in vortex-structure interaction, Paper IMECE 2002-32512, *Proceedings, 5th International Symposium on FSI, AE & FIV+N, ASME Int'l Mech. Engrg. Congress & Exhibition,* New Orleans, Louisiana, USA.

Mureithi, N.W., Rodriguez, M. 2005. Stability and bifurcation analysis of a forced cylinder wake. Paper IMECE 2005-79778, *Proceedings, ASME Int'l Mech. Engrg. Congress & Exhibition*, Orlando, Florida, USA.

Ongoren, A., Rockwell, D., 1988, Flow structure from an oscillating cylinder Part.2 Mode competition in the near wake. *Journal of Fluid Mechanics*. 191:225-245.

Rodriguez, M., Mureithi, N.W., 2006, Cylinder wake dynamics in the presence o stream-wise harmonic forcing, Paper PVP2006-ICPVT11-93847, *Proceedings, ASME PVP Division Conference*, Vancouver, BC, Canada.

Rodriguez, M., 2006, *Simulation et analyse numérique de la trainée en aval d'un cylindre soumis à des oscillations forcées,* MSc. Thesis, University of Montreal, Montreal Canada.

Williamson, C.H.K., Roshko, A. ,1988, Vortex formation in the wake of an oscillating cylinder. *Journal of Fluids and Structures*. **2**:355-381.

Figure 1. Vorticity field of the flow past the cylinder under forced oscillation for $V_r=5$ and (a)$A/D=0.25$, and (b) $A/D=0.35$.
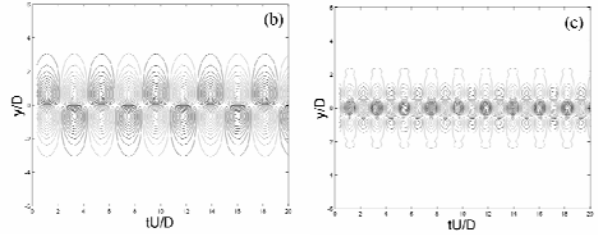
Figure 2 The first and second mode topos 10D downstream of the fixed cylinder.
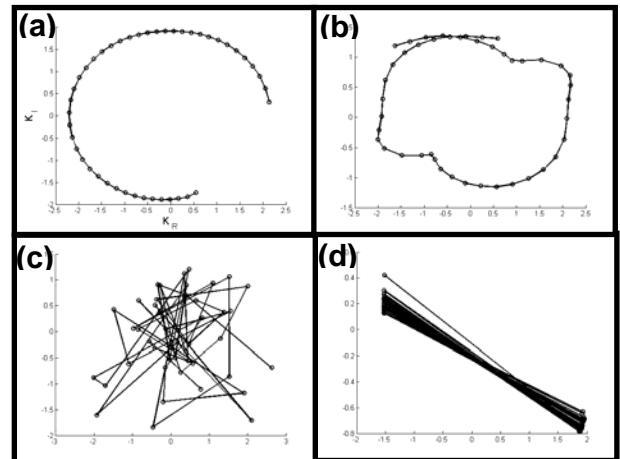
Figure 3 Poincare map relating the real and imaginary parts of successive mode K amplitudes for (a) $A/D=0$, (b) $A/D=0.05$, (c) $A/D=0.10$ and (d) $A/D=0.3$.
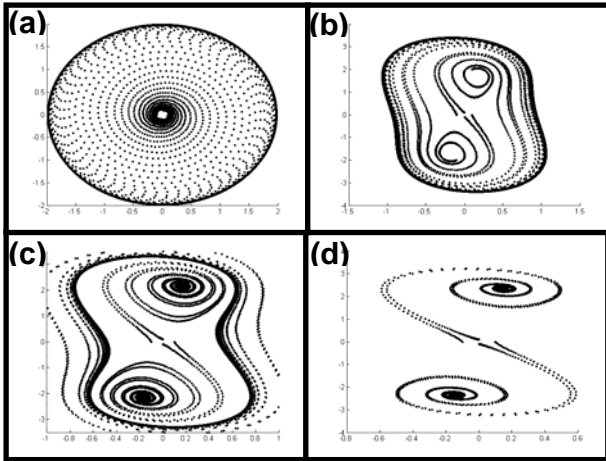
Figure 4 Poincare map relating the real and imaginary parts of successive mode K amplitudes for S-forcing amplitudes (a) S=0.025, (b) S=0.32325, (c) S=0.3325 and (d) S=0.3375.
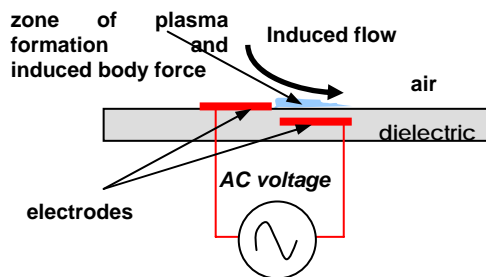
Figure 5 Basic concept of the single barrier dielectric discharge (SBD) plasma actuator.

Figure 6 Test cylinder in wind tunnel. Plasma actuators are mounted near the upper and lower separation lines.
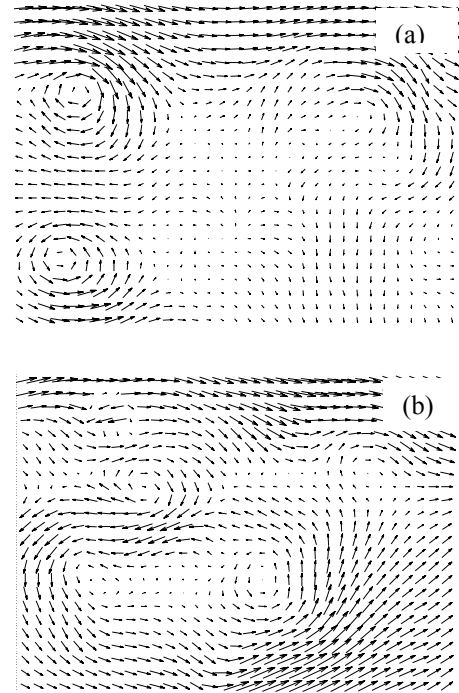
Figure 7 Examples of complex wake flow immediately downstream of cylinder, (a) vortex pair shedding, (b) alternate shedding with merging; plasma jet velocity 0.03 m/s.
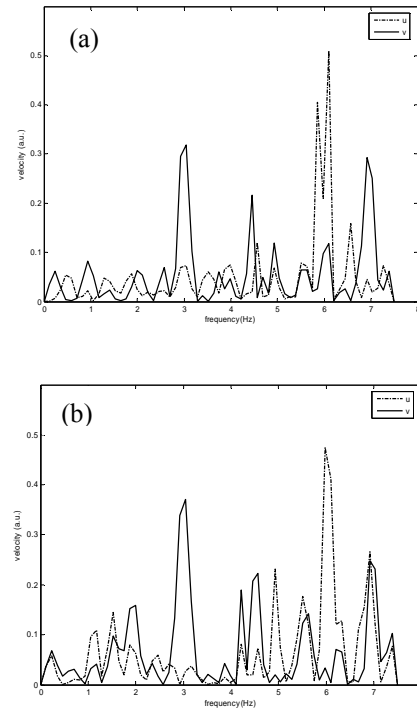
Figure 8 In flow and transverse velocity spectra at a location 0.75D off-center transversely and (a) 1.4D, (b) 2.4D downstream.